Available online at www.sciencedirect.com
SCIENCE DIRECT®
Journal of Solid State Chemistry 177 (2004) 1858–1866
JOURNAL OF SOLID STATE CHEMISTRY
http://elsevier.com/locate/jssc

Formation enthalpies of rare earth titanate pyrochlores

K.B. Helean,[a,b] S.V. Ushakov,[a] C.E. Brown,[a] A. Navrotsky,[a,*] J. Lian,[b] R.C. Ewing,[b,c] J.M. Farmer,[d] and L.A. Boatner[d]

[a] *Department of Chemical Engineering and Materials Science, Thermochemistry Facility, NEAT ORU, The University of California at Davis, One Sheilds Avenue, Davis, CA 95616, USA*
[b] *Department of Nuclear Engineering and Radiological Sciences, University of Michigan, Ann Arbor, MI 48109-2104, USA*
[c] *Department of Materials Science and Engineering, University of Michigan, Ann Arbor, MI 48109-2104, USA*
[d] *Oak Ridge National Laboratory, Solid State Division, Oak Ridge, TN 37831-6056, USA*

Received 9 October 2003; received in revised form 11 January 2004; accepted 15 January 2004

Abstract

High-temperature oxide melt solution calorimetry and Rietveld refinements of powder X-ray diffraction data were used to investigate the structure (*Fd3m*; $Z=8$) and energetics of a series of $RE_2Ti_2O_7$ (RE = Sm–Lu) compounds with the pyrochlore structure as well as $La_2Ti_2O_7$ with a layered perovskite-type structure. All of the *RE*-titanates were found to be stable in enthalpy with respect to their oxides. In the pyrochlore series, $Lu_2Ti_2O_7$ was least stable in enthalpy (ΔHf-ox at 298 K = -56.0 ± 4.0 kJ/mol); the most stable materials were Gd-, Eu-, and $Sm_2Ti_2O_7$ with ΔHf-ox at 298 K = -113.4 ± 2.7, -106.1 ± 4.2, -115.4 ± 4.2 kJ/mol, respectively. In general, as the radius ratio of the *A*- to *B*-site cations, R_A/R_B, decreases, the pyrochlore structure becomes less stable. The trend of ionic radius of the RE^{3+} cation vs. ΔHf-ox at 298 K is non-linear and approximately parallels the increasing "resistance" to ion-beam-induced amorphization as R_A/R_B decreases.

Keywords: Thermodynamics; Pyrochlore; Nuclear waste; Enthalpy

1. Introduction

Titanate pyrochlore, $A_2Ti_2O_7$, materials are important because of their potential use as solid electrolytes and mixed ionic/electronic conducting electrodes [1–9], catalysts [10], and ferroelectric/dielectric device components [11–14]. Pyrochlore is also a mineral, occurring in a wide variety of high-temperature geologic settings, including pegmatites and carbonatites, preferentially incorporating U (up to 30 wt%) and Th (up to 9 wt%) into the structure [15–18]. Most naturally occurring pyrochlores are at least partially metamict, i.e., amorphous due to the cumulative effects of the radioactive decay of ^{238}U, ^{235}U and ^{232}Th and their daughter products [19]. Because of the capacity of pyrochlore to incorporate actinides [20], pyrochlore and the structurally related monoclinic zirconolite, are the primary phases in the titanate-based waste form ceramics being investigated for the immobilization of plutonium from dismantled nuclear weapons [20–27]. Despite the broad interest in titanate pyrochlore, only estimated thermodynamic data have been reported previously in the literature [28]. In the present work, we report the results of a detailed thermochemical investigation of *RE*-titanate pyrochlore, $RE_2Ti_2O_7$ (where RE = Lu to Sm, or Y).

2. The pyrochlore structure

The pyrochlore, $A_2B_2O_7$, structure (*Fd3m*, $Z=8$), is an anion-deficient derivative of fluorite, AX_2 (*Fm3m*, $Z=1$), with two types of cations ordered on the *A*- and *B*-sites and one eighth of the anions removed. The structure can be envisioned as interpenetrating networks of BO_6 octahedra and A_2O chains of distorted cubes (Fig. 1) [29,30]. The general stoichiometry is given by $A_2B_2X_6X'$ where A = various large, low-valence cations such as Bi, In, Tl, Pb^{2+}, Sc, Cd, Hg^{2+}, Ca, Sr, Mn^{2+}, Sn^{2+} or RE (the lanthanides or Y) [29,30]. The *B*-site can be occupied by almost any transition metal capable

*Corresponding author. Fax: +530-752-9307.
E-mail address: anavrotsky@ucdavis.edu (A. Navrotsky).

0022-4596/$ - see front matter © 2004 Elsevier Inc. All rights reserved.
doi:10.1016/j.jssc.2004.01.009

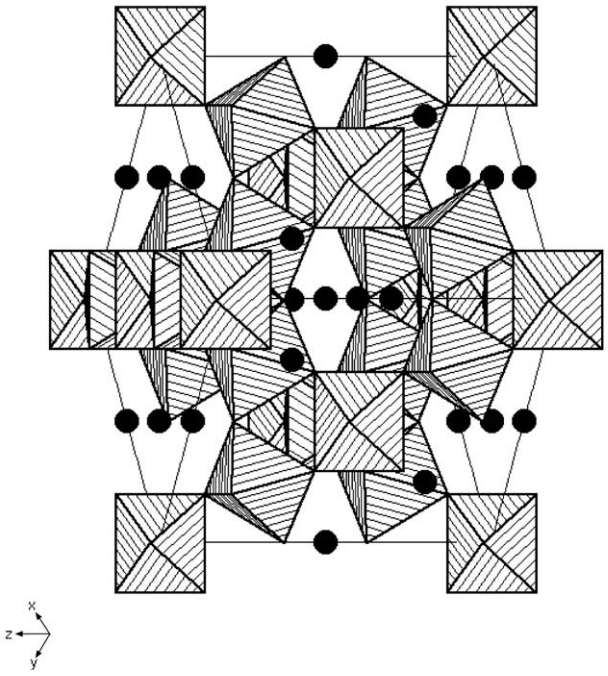

Fig. 1. The crystal structure of pyrochlore. TiO_6, SnO_6 or ZrO_6 octahedra share corners to form a framework structure. The large *A*-site cations (*RE*) occupy octahedral sites in the interlayer.

of octahedral coordination, e.g., Ru, Sn, Ti, Mo, Mn, V, Ir, Te, Bi, Pb, Sb, Zr, Hf, Mg, Cu, Zn, Al, Cr, Ga, Rh [29,30]. The ionic radii of the *A*- and *B*-site cations are typically in the ranges of $R_A = 0.087-0.151$ nm; $R_B = 0.040-0.078$ nm [29]. Empirically, the pyrochlore structure is stable when the radius ratio $R_A/R_B = 1.29-2.30$. Based on size and charge considerations, there are two common compositions: $(A^{3+})_2(B^{4+})_2X_6X'$, III–IV pyrochlore, and $(A^{2+})_2(B^{5+})_2X_6X'$, II–V pyrochlore [29,30]. Typical anions in pyrochlore are O^{2-}, F^-, and OH^- [29,30]. In the ideal pyrochlore structure the *B*-site cation is octahedrally coordinated by *X*, and *A* forms distorted cubes coordinated by *X* and *X'*. There are three anion sites, 48*f*, 8*a* and 8*b*, using Wyckoff's notation [31]. The 8*a*-anion site is unoccupied and surrounded by four *B*-site cations; the 8*b*-site is coordinated to four *A*-site cations and the 48*f*-site is coordinated with two *A*- and two *B*-site cations [8,9,31]. Taking the origin of the unit cell at the *B*-site, the pyrochlore anions form a perfect cubic arrangement if the positional parameter, *x*, for the O_{48f}, is equal to 3/8. When $x = 3/8$, the *A*-site cation polyhedron is a regular cube and the *B*-site polyhedron is a trigonally flattened octahedron [29,30]. As *x* decreases to 0.3125 the *B*-site becomes a regular octahedron, and the *A*-site distorts to form a trigonal scalenohedron [29,30]. For most pyrochlores $0.3125 < x < 0.375$ [29,30]. The *RE*-titanate pyrochlores lie in the range of $x = 0.322$ for $Gd_2Ti_2O_7$ to $x = 0.331$ for $Er_2Ti_2O_7$ [30].

Radius ratio constraints on pyrochlore formation ($R_A/R_B \geqslant 1.2$) result in *RE*-zirconate pyrochlore formation from La to Sm, *RE*-titanate pyrochlore formation from Lu to Sm, and the *RE*-stannate pyrochlores form across the entire series [30].

When the *A*-site in $A_2Ti_2O_7$ materials is occupied by La, Ce, Pr, or Nd, ($R_A/R_B > 1.78$), a monoclinic layered perovskite-type structure is adopted [32]. Layered perovskite-type structures can also be obtained by subjecting $RE_2Ti_2O_7$ pyrochlores to high pressure, e.g. $Eu_2Ti_2O_7$ [11,33]. $La_2Ti_2O_7$ is isostructural with $Ca_2Nb_2O_7$ ($P2_1$) [32,34]. The monoclinic modification undergoes a transformation to an orthorhombic structure ($Pbn2_1$) at ≈ 1053 K [34,35]. In both modifications, the coordination of the La cation is nine and the Ti coordination is six [32–35].

3. Previous work

Calculated formation enthalpies for $RE_2Ti_2O_7$ were reported based on extrapolations of measured *RE*-zirconate pyrochlore data [28,36]. Formation enthalpies of the *RE*-hafnates and zirconates were measured by Paputskii et al. (1974) by combustion in an adiabatic calorimeter [36]. Reznitskii (1993) used their experimental values to approximate the formation enthalpies for *RE*-zirconate and titanate pyrochlores [28]. Reznitskii used the enthalpy values reported by Paputskii et al. (1974) to derive *A* and *B* coefficients in the following equation:

$$\Delta H\text{f-ox} = A + B\sum(\delta H), \tag{1}$$

where $\Sigma(\delta H)$ is the sum of the enthalpy change associated with the change in coordination number of the cations upon formation of the compounds from their constituent oxides (Table 1) [28]. Using the derived *A* and *B* coefficients ($A = -132.8$; $B = 0.910$), the formation enthalpies for *RE*-titanate pyrochlores were calculated (Table 1) [28]. In the *RE*-zirconate and titanate pyrochlores, the coordination number, CN, for the *RE* is eight and for Zr and Ti it is six. In the *RE*-zirconate pyrochlores and fluorites, both the CN of *RE* and the CN of Zr change with respect to their oxides. For Zr^{4+} the CN changes from seven in the monoclinic oxide, ZrO_2, to six in the pyrochlore, $RE_2Zr_2O_7$, and eight in the fluorite, $(RE,Zr)O_{1.75}$. Reznitskii assigned an enthalpy change of 40 kJ/mol for the ZrO_7 to ZrO_6 coordination change; 20 kJ/mol for the ZrO_7 to ZrO_8 coordination change [28]. In *RE*-titanate pyrochlore, only the *RE* cation changes its coordination with respect to its oxide, Ti does not. In Reznitskii's calculation, *RE*-titanate pyrochlores are, thus, 20–40 kJ/mol more stable in enthalpy with respect to their oxides than their zirconate counterparts [28]. Reznitskii assumed that the substitution of RE^{3+} cations of variable size into the

Table 1
Drop solution enthalpies, ΔH_{ds}, used in the thermodynamic cycles

A-cation	Titanate structure	ΔH_{ds} titanates	ΔH_{ds} oxides[a]	ΔH_{f-ox}	ΔH_f^0	T_c (K)
La*	*M*	98.52±0.95	−191.70±2.46	−171.6±2.8	−3855.5±3.5	
Sm*	*P*	91.45±2.85	−153.62±2.86	−115.4±4.2 [−125]	−3808.5±4.8 [−3835]	1045
Eu*	*P*	94.03±3.56	−129.24±2.12	−106.1±4.2 [−120]	−3646.4±9.5 [−3671]	1080
Gd*	*P*	82.71±2.11	−148.54±1.60	−113.4±2.7 [−120]	−3822.5±4.7 [−3828]	1120
Tb	*P*	100.99±1.92	−125.58±2.40	−105.5±3.2 [−114]	−3851.2±9.0 [−3867]	970
Dy	*P*	98.28±2.70	−114.88±2.22	−97.8±3.6 [−111]	−3849.2±5.5 [−3862]	910
Ho	*P*	95.99±2.61	−111.72±3.68	−87.5±4.6 [−109]	−3848.4±6.8 [−3878]	850
Er	*P*	94.18±2.87	−105.26±2.48	−79.6±3.9 [−105]	−3852.7±4.5 [−3891]	804
Tm	*P*	80.82±2.13	−97.12±2.38	−79.1±3.3 [−101]	−3903.5±3.6 [−3878]	
Yb	*P*	86.55±2.04	−98.46±3.18	−70.5±3.9 [−100]	−3770.8±4.2 [−3802]	611
Lu	*P*	77.81±3.38	−96.90±1.90	−56.0±4.0 [−97]	−3819.0±8.6 [−3863]	480
Y*	*P*	83.05±0.74	−120.74±0.94	−86.2±1.5 [−106]	−3874.2±3.0 [−3899]	780
Ti			+58.92±0.82			

Errors are calculated as two standard deviations of the mean. Calorimetric data were collected using $3Na_2O \cdot 4MoO_3$ solvent at 976 K. (*) indicates sol–gel derived samples. Calculated values are in brackets [28] and critical amorphization temperatures (T_c) [44] are reported for comparison. $M = P2_1$ and $P = Fd3m$. All enthalpy values are reported in kJ/mol.

[a] Data taken from [53–55] .

titanate pyrochlore structure had little effect on the stability of the Ti–O framework. Therefore, the enthalpy changes associated with such substitutions are proportional to the enthalpy change due to the change in coordination of the RE^{3+} cation from its oxide (CN = 7) to the pyrochlore (CN = 8). Reznitskii's assumptions are supported by the observation that there is little change in the Ti–O bond length as a function of the ionic radii of the substituting RE^{3+} cation [29,30,37].

The purpose of the present study is to derive the enthalpies of formation for *RE*-titanate pyrochlores from measured solution enthalpies obtained using high-temperature oxide melt solution calorimetry.

4. Experimental

4.1. Sample synthesis and characterization

RE-titanate pyrochlore (*RE* = Eu to Lu) single crystals were grown by a flux technique at Oak Ridge National Laboratory (ORNL). The *RE*-titanate pyrochlores (*RE* = Sm, Eu, Gd, Y) prepared using the sol–gel method were provided by K.V.G. Kutty from the Indira Gandi Center for Atomic Research, India.

X-ray powder diffraction (XRD) data were collected using a Scintag PAD-V diffractometer with a Cu anode and an accelerating voltage of 45 kV over an angular range, $2\theta = 14-94^\circ$ and a 0.02° step size with a dwell time of 7 s. Unit cell parameters were refined by the Rietveld method using the general structure analysis system (GSAS) [38], the EXPGUI program [39], and the JADE software package [40]. Silicon was used as an internal standard [41]. All non-overlapping peaks from 14° to 94° 2θ were used in these refinements.

Quantitative chemical analysis data were collected using a Cameca SX50 electron microprobe (electron microprobe analysis, EMPA) with wavelength-dispersive spectroscopy (WDS), an accelerating voltage of 20 kV, a probe current of 10 nA, and a spot size of 1 μm. Energy dispersive spectroscopy (EDS), back-scattered electron imaging (BSE), and characteristic X-ray dot mapping were used to assess the sample chemical homogeneity. A ZAF correction was applied to the WDS data using the Cameca SX50 software.

A JEOL 2010F electron microscope with a field emission source was used at an accelerating voltage of 200 kV. High-resolution transmission electron microscopy (HRTEM) was used to assess the crystallinity and nanostructure of the pyrochlore samples. Samples were

prepared by polishing to form thin, electron-transparent wedges using an Ar^+ -ion mill.

4.1.1. Flux grown RE-titanate pyrochlore

Single crystals of the *RE*-titanate pyrochlores were grown using the high-temperature flux method [42,43]. $RE_2Ti_2O_7$ samples (*RE* = Eu–Lu) were grown at a fixed temperature of 1508 K from a lead-fluorite flux with a 10–1 weight ratio of PbF_2 flux to the component oxides ($RE_2O_3 + TiO_2$). Slow evaporation (130 h) of the flux at a fixed temperature of 1508 K resulted in pyrochlore crystal formation.

The powder X-ray diffraction data indicated that the flux grown samples were pyrochlore and contained no measurable impurities. Rietveld analyses of the diffraction data using GSAS [38] and EXPGUI [39] were used to calculate the cubic lattice parameters for the pyrochlore samples (Table 2). All results were generally consistent with but slightly larger than prior literature values [30] and reflect the gradual reduction of the unit cell volume in going from Eu to Lu. The O_{48f}, *x*, values for the single crystal titanate samples were refined using single crystal X-ray data (Table 2) [44].

EMPA indicated the presence of up to three-oxide weight percent lead—primarily in the form of externally adhered flux on the flux-grown single crystal *RE*-titanate samples (Table 3). Analyses were conducted on broken fragments of single crystals in the interior of each sample. At the level of detection of the microprobe ($\approx 1\,\mu m$) the measured lead internal impurity was not observed to be at the level of the adhered lead-fluoride flux that was generally present on every sample. This level of external lead contamination would contribute significantly to the measured solution enthalpies, thus, measures were taken to reduce or remove both adhered external lead flux and any internal lead impurities from the samples. To eliminate as much lead impurity as possible, the samples were heat treated to 1673–1723 K for 50 h. Rietveld refinements of powder X-ray diffraction data before and after heat treatment revealed that, in fact, some reduction in the unit cell parameter accompanied the loss of lead (Table 2). The reduction in lead content in the samples was confirmed by EMPA (Table 3). In addition to the presence of lead in the single crystals, each sample was found to be slightly non-stoichiometric (Table 3). Although these factors will impact the *x*-value as determined from the single-crystal refinements, it is unlikely that the change would be greater than the errors on these determinations (up to ± 0.00011 nm) (Table 2).

HRTEM was used to assess the sample crystallinity and examine the sample nanostructure (Fig. 2). HRTEM micrographs and selected area electron diffraction (SAED) patterns indicated that the flux grown *RE*-titanate pyrochlores single crystals had no apparent structural heterogeneities at the nanoscale.

4.1.2. Sol–gel grown RE-titanate pyrochlore

$RE_2Ti_2O_7$ samples (*RE* = Sm, Eu, Gd, Y) were prepared by a sol–gel method using an aqueous mixture of *RE*-nitrate and titanium chloride. These mixtures were treated with equal volumes of aqueous solutions of citric acid and ethylene glycol and allowed to evaporate to incipient dryness. The resulting powders were calcined at 973 K for 15 min and sintered at 1673 K in air for 10–30 h.

The powder X-ray diffraction data indicated that the sol–gel grown samples (*RE* = Sm, Eu, Gd, Y) were

Table 2
Cell parameters and the O_{48f}, *x*-values determined from Rietveld refinement of powder XRD data and single crystal structural refinements

A-site cation	Synthesis method	Cell param., nm (as received)	Cell param., nm (annealed)	Cell param., nm (ref.)[a]	O_{48f}, *x*-value	O_{48f}, *x*-value (ref.)[a]
RE-titanate pyrochlore						
Eu	Flux	1.02082(2)	1.02024(1)	1.0196	0.3267(3)	0.327
Gd	Flux	1.01930(2)	1.01703(2)	1.0185	0.3263(6)	0.322
Tb	Flux		1.01475(1)	1.0152	0.3281(5)	
Dy	Flux		1.01248(1)	1.0124	0.3275(5)	0.323
Ho	Flux	1.01045(2)	1.00986(1)	1.0100	0.3285(5)	
Er	Flux	1.00840(2)	1.00727(1)	1.0087	0.3278(8)	0.331
Tm	Flux	1.00694(6)	1.00537(2)	1.0054	0.3292(3)	
Yb	Flux	1.00425(2)	1.00204(1)	1.0030	0.3309(4)	
Lu	Flux	1.00341(10)	1.00069(1)	1.0018	0.3297(11)	0.330
Sm	Sol–gel	1.01933(6)	—	1.0233	—	0.327
Eu	Sol–gel	1.02129(3)	—	1.0196	—	0.327
Gd	Sol–gel	1.01860(5)	—	1.0185	—	0.322
Y	Sol–gel	1.00974(6)	—	1.0095	—	0.328

The flux-grown single crystal titanate samples were annealed at 1673–1723 K to remove Pb-impurities. Reference values, if available, are given for comparison [30].

[a] Data taken from [30].

Table 3
Results of EMPA-WDS analyses of the $RE_2Ti_2O_7$ pyrochlores. The standards used were RE–$REPO_4$, Pb–$PbZrO_3$, Ti–TiO_2

RE	Anneal[a]	TiO_2	RE_2O_3	PbO	Total	*N*	Formula[b]
RE-titanate pyrochlore							
Eu	As prep.	30.20±0.20	67.00±0.90	1.70±0.50	98.90±0.50	15	$Eu_{1.995}Ti_{1.984}Pb_{0.044}O_7$
	1673 K/50 h	30.40±0.48	67.13±0.53	0.17±0.21	97.70±0.64	15	$\mathit{Eu_{2.004}Ti_{1.995}Pb_{0.004}O_7}$
Gd	As prep.	29.80±0.30	66.80±1.50	3.30±1.30	99.90±0.60	11	$Gd_{1.963}Ti_{1.986}Pb_{0.077}O_7$
	1673 K/50 h	31.19±0.28	68.95±0.54	0.09±0.09	100.23±0.52	9	$\mathit{Gd_{1.970}Ti_{2.022}Pb_{0.002}O_7}$
Tb	As prep.	29.99±0.26	66.52±0.72	2.86±0.45	99.37±1.52	9	$Tb_{1.945}Ti_{2.007}Pb_{0.035}O_7$
	1673 K/50 h	30.60±0.33	68.37±0.31	0.18±0.26	99.15±0.26	9	$\mathit{Tb_{1.968}Ti_{2.022}Pb_{0.004}O_7}$
Dy	As prep.	29.20±0.55	67.39±0.71	2.30±0.36	98.89±1.27	10	$Dy_{1.977}Ti_{1.988}Pb_{0.056}O_7$
	1673 K/50 h	29.49±0.22	67.77±0.61	1.81±0.54	99.07±0.60	16	$Dy_{1.974}Ti_{1.997}Pb_{0.044}O_7$
	1723 K/50 h	29.17±0.51	69.74±0.35	0.24±0.18	99.15±0.60	8	$\mathit{Dy_{2.020}Ti_{1.979}Pb_{0.006}O_7}$
Ho	1673 K/50 h	29.93±0.22	69.22±0.66	0.31±0.37	99.46±0.38	6	$\mathit{Ho_{1.973}Ti_{2.017}Pb_{0.008}O_7}$
Er	1673 K/50 h	29.44±0.21	69.13±0.48	0.56±0.40	99.13±0.51	8	$\mathit{Er_{1.972}Ti_{2.013}Pb_{0.014}O_7}$
Tm	1673 K/50 h	26.43±1.94	71.58±0.96	0.83±0.69	98.84±0.77	6	$Tm_{2.128}Ti_{1.893}Pb_{0.022}O_7$
	1723 K/50 h	25.32±2.40	72.70±2.39	0.13±0.11	98.15±0.96	12	$\mathit{Tm_{2.203}Ti_{1.846}Pb_{0.003}O_7}$
Yb	1673 K/50 h	27.48±1.60	69.56±1.79	0.76±0.59	97.80±0.69	11	$\mathit{Yb_{2.026}Ti_{1.971}Pb_{0.020}O_7}$
Lu	1673 K/50 h	28.29±0.40	69.84±0.48	0.08±0.08	98.21±0.54	8	$\mathit{Lu_{1.989}Ti_{2.006}Pb_{0.002}O_7}$
La[c]	N/A[d]	32.62±0.17	66.82±0.22	—	99.45±0.32	12	$\mathit{La_{2.005}Ti_{1.996}O_7}$
Sm[c]	N/A	32.78±0.23	65.54±0.31	—	98.33±0.25	12	$\mathit{Sm_{1.901}Ti_{2.075}O_7}$
Eu[c]	N/A	30.81±0.42	67.69±0.60	—	98.50±0.65	12	$\mathit{Eu_{1.997}Ti_{2.002}O_7}$
Gd[c]	N/A	30.54±0.24	69.45±0.47	—	96.99±0.64	15	$\mathit{Gd_{2.002}Ti_{1.998}O_7}$
Y[c]	N/A	41.12±0.84	56.71±0.67	—	97.83±0.78	12	$\mathit{Y_{1.972}Ti_{2.021}O_7}$

[a] As prep.—"as prepared" single crystals flux-grown at 1508 K. For further annealing, crystals were powdered in mortar and pestle.
[b] The samples used for drop solution calorimetry are in *italics*.
[c] Samples prepared using sol–gel techniques.
[d] N/A-heat treatment of the sol–gel derived samples was not necessary.

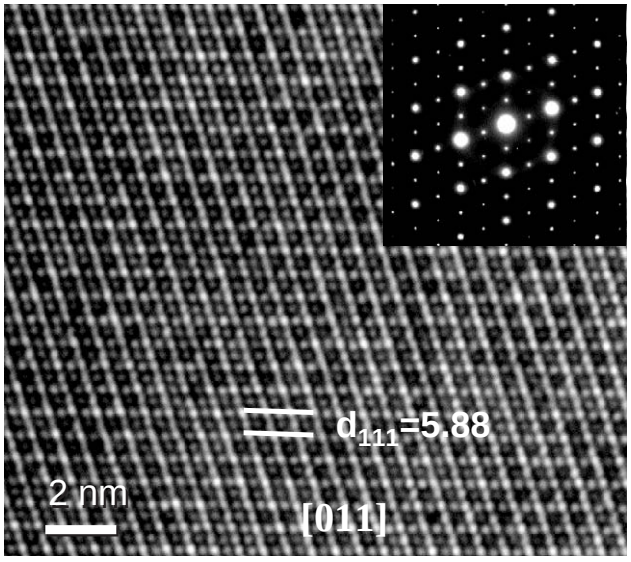

Fig. 2. HRTEM images with selected area electron (SAED) diffraction patterns (inset) of $Gd_2Ti_2O_7$ down the [0 1 1] zone. Features in the micrograph and diffraction pattern are consistent with the pyrochlore structure. All *RE*-titanate pyrochlore samples examined gave similar results.

pyrochlore and contained no measurable impurities. The $La_2Ti_2O_7$ was monoclinic with the $Ca_2Nb_2O_7$ structure. Rietveld analyses of the diffraction data using GSAS [38] and EXPGUI [39] were used to calculate the cubic lattice parameters for the pyrochlore samples (Table 2). All of the results were consistent with literature values [30]. Conventional powder XRD does not have the resolution to allow for the accurate determination of oxygen positional parameters, thus, the x-values for the sol–gel-grown samples were taken from the literature (Table 2) [30].

The EMPA-WDS indicated that all the sol–gel-prepared samples were non-stoichiometric (Table 3). For La, Eu, Gd, and Y-titanates, the non-stoichiometry is insignificant because the enthalpies associated with such small deviations from stoichiometry are well within the experimental error of the calorimetry (1.5–4.6 kJ/mol). Thus, these samples are treated as stoichiometric $RE_2Ti_2O_7$ in all of the thermodynamic calculations. The Sm-bearing sample is significantly non-stoichiometric with a chemical formula of $Sm_{1.901}Ti_{2.075}O_7$. The pyrochlore structure has been shown to tolerate non-stoichiometry at high temperature [45]. All relevant thermodynamic data were corrected to reflect the non-stoichiometry of this sample (see Table 4). No impurities were observed in the sol–gel grown samples at the level of resolution of the electron microprobe ($\approx 1\,\mu m$).

High-resolution transmission electron microscopy (HRTEM) was used to assess the sample crystallinity and examine the sample nanostructure. HRTEM micrographs and selected area electron diffraction (SAED) patterns indicated that the sol–gel synthesized bulk *RE*-titanate powders were completely crystalline at the nanoscale.

Table 4
Thermodynamic cycle used in calculating enthalpies of formation from the oxides (kJ/mol) for the titanate pyrochlore samples where $A = RE$, $B = \mathrm{Ti}$ and x, y, z were determined using EMPA-WDS

ΔH_{ds} (kJ/mol)	Reaction
ΔH_1	$A_xB_y\mathrm{Pb}_z\mathrm{O}_{7\ (s,\ 298\,K)} \rightarrow [(x/2)A_2\mathrm{O}_3 + yBO_2 + z\mathrm{PbO}]_{(solution,\ 976\,K)}$
ΔH_2	$A_2\mathrm{O}_{3(s,\ 298\,K)} \rightarrow A_2\mathrm{O}_{3(solution,\ 976\,K)}$ [a]
ΔH_3	$BO_{2(s,\ 298\,K)} \rightarrow BO_{2(solution,\ 976\,K)}$
ΔH_4	$\mathrm{PbO}_{(s,\ 298\,K)} \rightarrow \mathrm{PbO}_{(solution,\ 976\,K)}$ [b]
ΔH^0f-ox	
$A_xB_y\mathrm{Pb}_z\mathrm{O}_{7(s,298\,K)} = -\Delta H_1 + (x/2)\Delta H_2 + y\Delta H_3 + z\Delta H_4$	

Errors are propagated assuming independent, linear combinations.
[a] Data taken from [54,55].
[b] Data taken from [67].

4.2. Calorimetric methods

High-temperature oxide melt solution calorimetry [46,47] was used to measure the drop solution enthalpies of the pyrochlore samples plus their binary oxide components. A Tian–Calvet twin microcalorimeter was used, and the description of its design and operation are described in detail elsewhere [46,47]. Prior to calorimetry, the powder samples were dried at 973 K for a minimum of 1 h. The rare earth sesquioxide powders were dried at 1473 K, vacuum-sealed in a desiccator, and handled in an Ar-filled glove box to prevent hydration and carbonation of these samples. The solvent used in this study was $3\mathrm{Na}_2\mathrm{O} \cdot 4\mathrm{MoO}_3$, at 976 K. Drop solution enthalpies, ΔH_{ds}, were measured by dropping pellets (≈ 5 mg) of the powdered samples from room temperature into the solvent at the calorimeter temperature. Thus, these measurements consist of two components, the heat content of the sample, ${}_{298}\int^{T} C_p\,dT$, and the heat of solution, ΔH_s. Oxygen was bubbled through the melt to aid in the dissolution of the pellets and to provide high oxygen fugacity [48]. The calorimeters were calibrated using the heat content of α-$\mathrm{Al}_2\mathrm{O}_3$ [49]. The measured values of the drop solution enthalpies were used in the appropriate thermodynamic cycles to calculate the enthalpies of formation from the oxides. Reference data for the binary oxides were used to calculate the enthalpies of formation from elements [50].

5. Results

Drop solution experiments using a $3\mathrm{Na}_2\mathrm{O} \cdot 4\mathrm{MoO}_3$ solvent at 976 K were conducted for TiO_2, rutile, $RE_2\mathrm{O}_3$ where $RE = \mathrm{La–Lu}$ (excluding Ce, Pm, Pr) plus Y, and the pyrochlore samples (Table 1). The ΔH_{ds} value for TiO_2 was consistent with previously reported values [51–53]. The ΔH_{ds} data for the *RE*-sesquioxides were previously reported and shown to be reliable through the application of multiple thermodynamic cycles and crosschecks [54,55]. A recent thermochemical investigation of La-bearing materials revealed an error in the previously reported calorimetric data for $\mathrm{La}_2\mathrm{O}_3$ [56]. In previous work, the sample partially hydrated during transfer to the glove box resulting in a more endothermic value for ΔH_{ds} $\mathrm{La}_2\mathrm{O}_3$. The more recent work made use of a modified vacuum tube that prevented hydration. The corrected value for ΔH_{ds} $\mathrm{La}_2\mathrm{O}_3$ is: -225.10 ± 3.16 kJ/mol and is used in all subsequent thermodynamic calculations [56].

The calorimetric data were used in thermodynamic cycles (Table 4) to calculate enthalpies of formation of the *RE*-titanates from the oxides, ΔH^0f-ox (kJ/mol) (Table 1). The standard enthalpies of formation, ΔH_f^0, were also calculated (Table 1).

6. Discussion

6.1. Comparison to previous reported data

The measured formation enthalpies, ΔHf-ox, for the $RE_2\mathrm{Ti}_2\mathrm{O}_7$ pyrochlores are consistent with the previously reported calculated data (Fig. 4) [28]. In general, a plot of the radius ratio of the *A* to *B*-site cations against the formation enthalpies shows a decrease in stability with respect to the oxides as R_A/R_B decreases (Fig. 3) [57]. This is consistent with observations that pyrochlore has an increasing tendency to disorder to a defect fluorite structure as R_A/R_B decreases [30]. The implication is that the related fluorite structure becomes more energetically competitive. There is reasonable agreement between the calculated and measured values for the RE^{3+} ions from Gd to Sm [28]. From $RE^{3+} = \mathrm{Dy–Lu}$, the data sets diverge with the measured data becoming more endothermic (Fig. 4). This discrepancy may be explained in part by increasing residual disorder in the

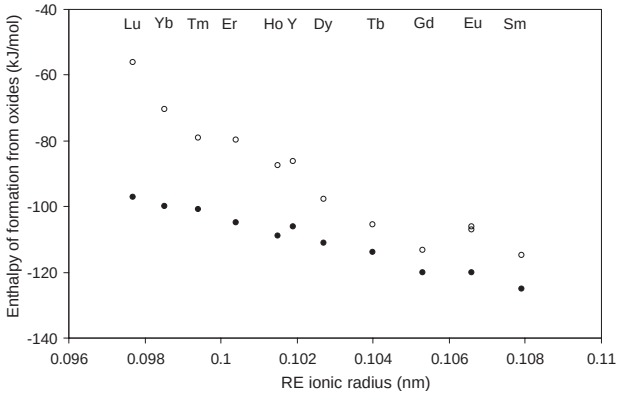

Fig. 3. The enthalpy of formation from the oxides, ΔH^0f-ox, of *RE*-titanate pyrochlores (closed circles) vs. the cation radius ratio, R_A/R_B. All pyrochlores are stable relative to an oxide assemblage with increasing stability as R_A/R_B increases. The measured data (open circles) are more endothermic than the previously reported theoretical values.

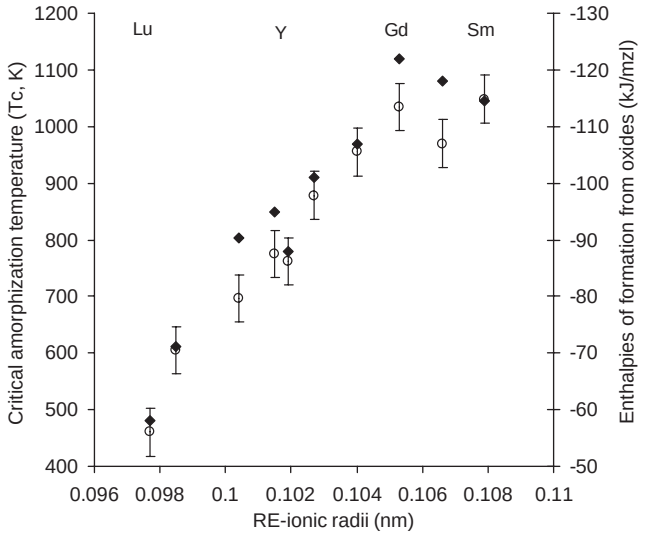

Fig. 4. The correlation between the formation enthalpies from the oxides, ΔH^0f-ox, and the critical amorphization temperature, T_c (K). The open symbols correspond to the enthalpy data and the closed symbols represent T_c (K).

titanate pyrochlores from Dy to Lu [58–60]. Partial disorder via the mechanism of cation anti-site defect formation would result in a decrease in pyrochlore stability, i.e., in more endothermic formation enthalpies. Recent studies endeavored to quantify the energetics of defect formation in the pyrochlore structure [61–64]. Two important observations were made: the most stable defect in pyrochlore is the cation anti-site defect and the energy required to form this defect decreases linearly as R_A/R_B decreases. This is consistent with observations that as R_A/R_B decreases, residual cation disorder increases [58–60]. This explanation alone can not account for the large ($\approx$40 kJ/mol) difference in the $Lu_2Ti_2O_7$ data. The assumption of the Reznitskii model that the effects of *RE* substitution in the titanate pyrochlore may be approximated by the zirconate pyrochlore data may not account for differences in the bonding of the Zr–O and Ti–O framework induced by the *RE* substitutions.

6.2. Formation enthalpies vs. susceptibility to radiation damage

A systematic ion beam irradiation study has been completed using the same samples as those employed in this study [44]. Single crystals of $A_2Ti_2O_7$ (A = Sm–Lu) were irradiated by 1 MeV Kr^+ ions over a temperature range from 293 to 1073 K using the HVEM-IVEM Tandem Facility at Argonne National Laboratory. The microstructural evolution was characterized using in situ HRTEM, and critical amorphization temperatures (T_c) were determined [44]. There is a remarkable consistency between the measured ΔHf-ox and the "resistance" to radiation damage as indicated by the critical amorphization temperature, T_c, for the $RE_2Ti_2O_7$ pyrochlores when plotted against the RE^{3+} ionic radii (Fig. 4) [44]. The critical amorphization temperature is the temperature above which annealing processes dominate the damage process, and the crystal can no longer be amorphized [44]. The lower the T_c for a material, the higher the radiation damage "resistance" because annealing removes the damage domains at relatively lower temperatures. The T_c curve reaches a maximum for $Gd_2Ti_2O_7$ (T_c = 1120 K) indicating that this material is the least "resistant" to radiation damage (Fig. 4) [44]. Among the *RE*-titanates, $Lu_2Ti_2O_7$, has the lowest T_c = 480 K and is the most radiation "resistant" [44].

Several recent studies have suggested that the ease with which a pyrochlore can form cation anti-site defects, i.e. the ease with which the material can disorder among the *A*- and *B*-sites and form a defect fluorite structure, is a critical parameter in predicting its radiation resistance [58–64]. This is generally consistent with the observation of significant residual disorder and a low T_c for $Lu_2Ti_2O_7$. However, these models focus on ionic radii and fail to take into account changes in bond type and the electronic configurations of the substituting *A*-site cation [44] and, thus, can not explain the deviations from linearity for T_c observed for Gd-, Eu-, and $Sm_2Ti_2O_7$ (Fig. 4). A similar non-linear trend is observed in the enthalpy data (Fig. 4).

A linear relationship between ΔHf-ox (kJ/mol) and T_c (K) describes $\approx$96% of the variation in the titanate pyrochlore data (Fig. 5) [44]. In general, as the propensity of the material to disorder increases, the radiation damage resistance increases, and the pyrochlore structure becomes less stable in enthalpy with respect to the oxides. The residual disorder that was inferred from the radiation effects study [44] would have the effect of destabilizing the $Lu_2Ti_2O_7$ pyrochlore in

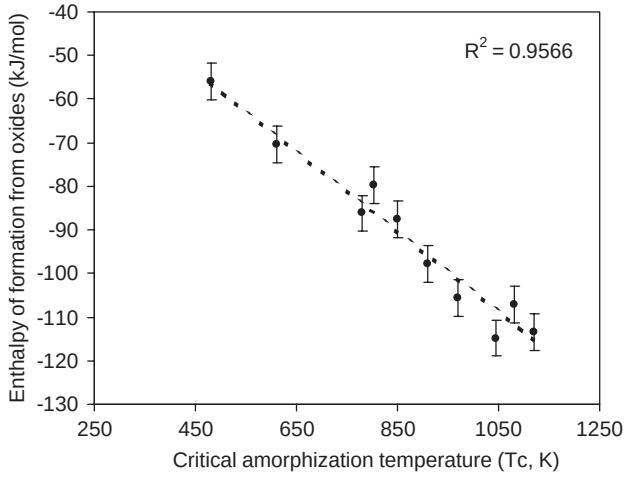

Fig. 5. A plot of the enthalpy of formation from the oxides, ΔHf-ox (kJ/mol), of the *RE*-titanate pyrochlores vs. the critical amorphization temperature, T_c (K). The trend is linear with an $R^2 \approx 96\%$.

enthalpy with respect to the oxides as the fluorite structure begins to compete energetically. The change in slope of the T_c and ΔHf-ox curve at $Gd_2Ti_2O_7$ may be correlated to structural features indicating that the Ti–O_{48f} bond is more covalent resulting in the smallest x value in the $RE_2Ti_2O_7$ series (Table 2; Fig. 4) [44]. For the *RE*-titanate pyrochlores, substituting Gd for Tb increases the stability by, presumably, better satisfying the bond requirements of the *A*-site. This stabilization effect may continue until the *A*-site cation becomes too large and begins to have a destabilization effect as indicated by the flattening of the enthalpy curve from Gd to Sm. This is consistent with the phase transformation associated with the substitution of RE^{3+} with ionic radii larger than Sm that results in the formation of a layer perovskite-type structure [11,32–35]. Similar effects have been observed in other *RE*-bearing complex ceramics and reveal a potential pitfall in linear extrapolations of thermodynamic data [65,66].

6.3. Transition enthalpy from pyrochlore to layered perovskite for $La_2Ti_2O_7$

$La_2Ti_2O_7$ forms in a monoclinic ($P2_1$) layered perovskite-type (LP) structure. The ΔHf-ox ($La_2Ti_2O_7$) is -206.0 ± 4.2 kJ/mol. Not surprisingly, this value is significantly more exothermic than a linear extrapolation of the $RE_2Ti_2O_7$ pyrochlore data would predict (Fig. 6). The difference between the predicted ΔHf-ox for the hypothetical pyrochlore structure and the ΔHf-ox for the monoclinic structure gives the transition enthalpy for the phase change, $\Delta H_{t-P/LP}$. Removing from consideration the samples that were shown to contain either significant residual disorder ($Lu_2Ti_2O_7$) or a change in the predominant bond type as inferred from structural data (Gd-, Eu-, $Sm_2Ti_2O_7$), a simple linear relationship is defined by

$$\Delta H\text{f-ox(pyrochlore)} = -378.12(R_A/R_B) + 545.74. \quad (2)$$

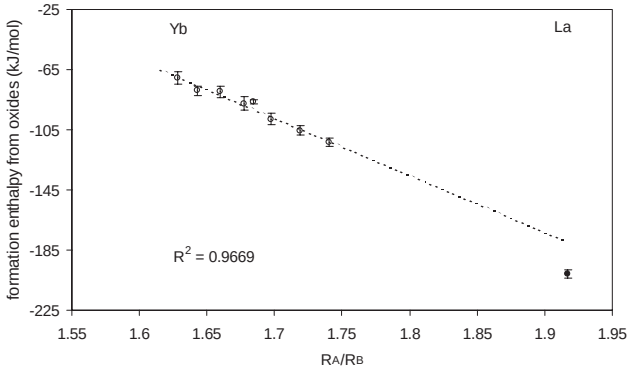

Fig. 6. The linear trend used to calculate the transition enthalpy, $\Delta H_{t-P/LP}$, from pyrochlore to the layered perovskite structure (closed circle) for $La_2Ti_2O_7$.

Approximately 97% of the variation in the data is explained by this linear model (Fig. 6). For $La_2Ti_2O_7$, $R_A/R_B = 1.92$ and the predicted ΔHf-ox(pyrochlore) $= -180 \pm 10$ kJ/mol. The $\Delta H_{t-P/LP}$ ($La_2Ti_2O_7$) $= -26 \pm 10$ kJ/mol. The prior discussion section highlights the problems with simple linear extrapolations. The $\Delta H_{t-P/LP}$ ($La_2Ti_2O_7$) should only be considered as a first approximation. In addition, assessing the error on this calculation is difficult and is arbitrarily set at 10 kJ/mol.

7. Conclusions

All of the $RE_2Ti_2O_7$ samples were stable in enthalpy with respect to their oxides. The general trend of decreasing stability with decreasing R_A/R_B is consistent with an increasing propensity to disorder and a more energetically favorable fluorite structure. Deviations in linearity in the enthalpy data are consistent with the observed trends in radiation damage "resistance" as determined by shifts in the critical temperature, that is the temperature above which the material cannot be amorphized by an ion beam irradiation. Significant residual disorder of the $Lu_2Ti_2O_7$ sample is inferred from the ease with which it disordered during ion bombardment and its low critical amorphization temperature, $T_c = 480$ K. This is consistent with the enthalpy data. A change in the enthalpy slope at $Gd_2Ti_2O_7$ corresponds to a change in slope of T_c that is attributed to small values of the O_{48f} positional parameter, x, and inferred increased covalency of the Ti–O_{48f} bond. A first approximation of the transition enthalpy from a pyrochlore to a layered perovskite-type structure for $La_2Ti_2O_7$ was made giving $\Delta H_{t-P/LP} \approx -26 \pm 10$ kJ/mol.

Acknowledgments

Financial support was provided by the University of California at Davis and by the Office of Basic Energy Sciences, DOE grant DE-FG02-97ER45656 (RCE). Oak Ridge National Laboratory is managed by UT-Battelle, LLC, for the US Department of Energy under contract DE-AC05-00OR22725.

References

[1] S. Kramer, M. Spears, H.L. Tuller, Solid Oxide Fuel Cells Symp. Proc. 93–94 (1993) 119.
[2] V.F. Zinchenko, V.D. Kozlov, G.A. Teterin, I.M. Minaev, Inorg. Mater. 25 (3) (1989) 391.
[3] T.H. Yu, H.L. Tuller, Ceram. Trans. 65 (1995) 3.
[4] S.A. Kramer, H.L. Tuller, Solid State Ion. 82 (1995) 15.

[5] B.J. Wuensch, K.W. Eberman, JOM—J Min. Met. Mater. Soc. 52 (2000) 19.
[6] P.K. Moon, H.L. Tuller, Solid State Ion. 28-30 (1988) 470.
[7] R.E. Williford, W.J. Weber, R. Devanathan, J.D. Gale, J. Electroceram. 3 (1999) 409.
[8] P.J. Wilde, C.R.A. Catlow, Solid State Ion. 112 (1998) 173.
[9] P.J. Wilde, C.R.A. Catlow, Solid State Ion. 112 (1998) 185.
[10] J. Christopher, C.S. Swamy, J. Mater. Sci. 26 (18) (1991) 4966.
[11] A.M. Sych, S.U. Stefanovich, U.A. Titov, T.N. Bondarenko, Mel'nik VM. Inorg. Mater. 27 (12) (1991) 2229.
[12] J.H. Lee, Y.M. Chiang, J. Electroceram. 6 (1) (2001) 7.
[13] R.J. Cava, J. Mater. Chem. 11 (1) (2001) 54.
[14] J.P. Mercurio, A. Lambachri, B. Frit, Sci. Ceram. Symp. Proc. 14 (1988) 967.
[15] G.R. Lumpkin, E.M. Foltyn, R.C. Ewing, J. Nucl. Mater. 129 (1986) 113.
[16] G.R. Lumpkin, Y. Eyal, R.C. Ewing, J. Mater. Res. 3 (2) (1988) 357.
[17] G.R. Lumpkin, R.C. Ewing, Amer. Mineral. 118 (1992) 393.
[18] G.R. Lumpkin, J. Nucl. Mater. 289 (2001) 136.
[19] B.C. Chakoumakos, R.C. Ewing, .Res Mater, Soc. Symp. Proc. 44 (1985) 641.
[20] A.E. Ringwood, S.E. Kesson, N.G. Ware, W. Hibberson, A. Major, Nature 278 (1979) 219.
[21] G.R. Lumpkin, R.C. Ewing, Phys. Chem. Mineral. 16 (1988) 2.
[22] R.C. Ewing, Science 192 (1976) 1336.
[23] A. Jostons, E.R. Vance, D.J. Mercer, V.M. Oversby, .Res Mater, Soc. Symp. Proc. 53 (1995) 775.
[24] E.R. Vance, B.D. Begg, R.A. Day, C.J. Ball, .Res Mater, Soc. Symp. Proc. 53 (1995) 767.
[25] N.K. Kulkarni, S. Sampath, V. Venugopal, J. Nucl. Mater. 281 (2000) 248.
[26] A. Jostons, E.R. Vance, B. Ebbinghaus, Proceedings of the International Conference on Future Nuclear Systems Global 99, American Nuclear Society CDROM, 1999.
[27] W.J. Weber, R.C. Ewing, C.R.A. Catlow, T. Diaz de la Rubia, L.W. Hobbs, C. Kinoshita, Hj. Matzke, A.T. Motta, M. Nastasi, E.H.K. Salje, E.R. Vance, S.J. Zinkle, J. Mater. Res. 13 (6) (1998) 1434.
[28] L.A. Reznitskii, Mosk. Neorg. Mater. 29 (9) (1993) 1310.
[29] B.C. Chakoumakos, J. Solid State Chem 53 (1984) 120.
[30] M.A. Subramanian, G. Aravamudan, G.V.S. Rao, Prog. Solid State Chem. 15 (1983) 55.
[31] International Tables for Crystallography, Vol. 1A.
[32] U. Balachandran, N.G. Eror, J. Mater. Res. 4 (6) (1989) 1525.
[33] I.M. Maister, Inorg. Mater. 19 (9) (1984) 1335.
[34] M. Gasperin, Acta Crystallogr. B 31 (1975) 2129.
[35] A.V. Prasadarao, U. Selvaraj, S. Komarneni, A.S. Bhalla, J. Am. Ceram. Soc. 75 (10) (1992) 2697.
[36] Y.N. Paputskii, V.A. Krzhizhanovskaya, V.B. Glushkova, Neorg. Mater. 10 (8) (1974) 1551.
[37] O. Knop, F. Brisse, L. Castelliz, Can. J. Chem. 47 (1969) 971.
[38] A.C. Larson, R.B. von Dreele, LANSCE, MS-H805, Los Alamos, NM, 1994.
[39] B.H. Toby, J. Appl. Crystallogr. 34 (2001) 210.
[40] JADE, Materials Data, Inc., Livermore, CA, 1997.
[41] NBS Certificate: Standard Reference Material 640b, 1987.
[42] R.S. Feigelson, J. Am. Ceram. Soc. 47 (1964) 257.
[43] M. Rappaz, L.A. Boatner, M.M. Abraham, J. Chem. Phys. 73 (1980) 1095.
[44] J. Lian, J. Chen, L.M. Wang, R.C. Ewing, J.M. Farmer, L.A. Boatner, K.B. Helean, Phys. Rev. B. (2003), in press.
[45] C.R. Stanek, L. Minervini, R.W. Grimes, J. Am. Ceram. Soc. 85 (11) (2002) 2792.
[46] A. Navrotsky, Phys. Chem. Min. 2 (1977) 89.
[47] A. Navrotsky, Phys. Chem. Min. 24 (1997) 22.
[48] A. Navrotsky, J. Therm. Anal. Calorim. 57 (1999) 653.
[49] NBS Certificate: Standard Reference Material 720, April 1982.
[50] R.A. Robie, B.S. Hemingway, US Geol. Surv. Bull. (1995) 2131.
[51] A. Navrotsky, O.J. Kleppa, J. Am. Ceram. Soc. 50 (1967) 626.
[52] A. Navrotsky, O.J. Kleppa, J. Inorg. Nucl. Chem. 30 (1968) 479.
[53] K.B. Helean, A. Navrotsky, E.R. Vance, M.L. Carter, B. Ebbinghaus, O. Krikorian, J. Lian, L.M. Wang, J.G. Catalano, J. Nucl. Mater. 303 (2001) 226.
[54] S.V. Ushakov, K.B. Helean, A. Navrotsky, L.A. Boatner, J. Mater. Res. 16 (9) (2001) 2623.
[55] K.B. Helean, A. Navrotsky, J. Therm. Anal. Calor. 69 (2002) 751.
[56] J. Cheng, A. Navrotsky, J. Mater. Res. 2003, in press.
[57] R.D. Shannon, Acta Crystallogr. A32 (1976) 751.
[58] C. Heremans, B.J. Wuensch, J.K. Wuensch, J.K. Staik, E. Prince, J. Solid State Chem. 117 (1995) 108.
[59] S.X. Wang, L.M. Wang, R.C. Ewing, G.S. Was, G.R. Lumpkin, Nucl. Instrum. Methods B 148 (1999) 704.
[60] S.X. Wang, B.G. Begg, L.M. Wang, R.C. Ewing, W.J. Weber, K.V.G. Kutty, J. Mater. Res. 14 (1999) 4470.
[61] K.E. Sickafus, L. Minervini, R.W. Grimes, J.A. Valdez, M. Ishimaru, F. Li, K.J. McClellan, T. Hartmann, Science 289 (2000) 748.
[62] L. Minervini, R.W. Grimes, K.E. Sickafus, J. Am. Ceram. Soc. 83 (2000) 1873.
[63] R.E. Williford, W.J. Weber, R. Devanathan, J.D. Gale, J. Electroceram. 3 (1999) 409.
[64] A. Charties, C. Meis, W.J. Weber, L.R. Corrales, Phys. Rev. B. 65 (2002) 134116.
[65] A.S. Risbud, K.B. Helean, M.C. Wilding, P. Lu, A. Navrotsky, J. Mater. Res. 16 (2001) 2780.
[66] A. Navrotsky, Ceram. Trans. 119 (2001) 137.
[67] J. Majzlan, A. Navrotsky, B.J. Evans, Phys. Chem. Mineral. 29 (2002) 515.